Journal of Biomedical Optics 11(4), 041121 (July/August 2006)

Quantitative evaluation of optical coherence tomography signal enhancement with gold nanoshells

Anant Agrawal
US Food and Drug Administration
Center for Devices and Radiological Health
Optical Diagnostics Laboratory
12725 Twinbrook Parkway, HFZ-130
Rockville, Maryland 20852
E-mail: anant.agrawal@fda.hhs.gov

Stanley Huang
Johns Hopkins University
Department of Biomedical Engineering
318 Clark Hall
3400 N. Charles Street
Baltimore, Maryland 21218

Alex Wei Haw Lin
Min-Ho Lee
Rice University
Department of Bioengineering
PO Box 1892, MS-142
Houston, Texas 77251-1892

Jennifer K. Barton
The University of Arizona
Division of Biomedical Engineering
1230 E Speedway Boulevard
Tucson, Arizona 85721-0104

Rebekah A. Drezek
Rice University
Department of Bioengineering
PO Box 1892, MS-142
Houston, Texas 77251-1892

T. Joshua Pfefer
US Food and Drug Administration
Center for Devices and Radiological Health
Optical Diagnostics Laboratory
12725 Twinbrook Parkway, HFZ-130
Rockville, Maryland 20852

Abstract. Nanoshell-enhanced optical coherence tomography (OCT) is a novel technique with the potential for molecular imaging and improved disease detection. However, optimization of this approach will require a quantitative understanding of the influence of nanoshell parameters on detected OCT signals. In this study, OCT was performed at 1310 nm in water and turbid tissue-simulating phantoms to which nanoshells were added. The effect of nanoshell concentration, core diameter, and shell thickness on signal enhancement was characterized. Experimental results indicated trends that were consistent with predicted optical properties—a monotonic increase in signal intensity and attenuation with increasing shell and core size. Threshold concentrations for a 2-dB OCT signal intensity gain were determined for several nanoshell geometries. For the most highly backscattering nanoshells tested—291-nm core diameter, 25-nm shell thickness—a concentration of 10^9 nanoshells/mL was needed to produce this signal increase. Based on these results, we discuss various practical considerations for optimizing nanoshell-enhanced OCT. Quantitative experimental data presented here will facilitate optimization of OCT-based diagnostics and may also be relevant to other reflectance-based approaches as well. [DOI: 10.1117/1.2339071]

Keywords: image enhancement; imaging coherence; optical properties.

Paper 05280SSR received Sep. 30, 2005; revised manuscript received Feb. 24, 2006; accepted for publication Apr. 11, 2006; published online Sep. 6, 2006. This paper is a revision of a paper presented at the SPIE Conference on Optical Coherence Tomography and Coherence Techniques II, Jun. 2005, Munich, Germany. The paper presented there appears (unrefereed) in SPIE proceedings Vol. 5861.

1 Introduction

Optical coherence tomography (OCT) has received considerable attention as a revolutionary biomedical imaging method since its introduction just over a decade ago.[1] However, only recently have researchers begun to explore the possibilities of improving OCT image quality in biological tissue with exogenous contrast agents, many of which can provide molecular contrast.[2–13] For example, air-filled microbubbles[2] and engineered microspheres[3] have been used to enhance the intensity of backscattered light from the tissue for OCT imaging. Near-infrared dyes that are spectrally active have been shown to enhance spectroscopic OCT images.[4]

Metal nanoparticles—including homogeneous nanospheres,[14] nanoshells,[15–17] and nanocages[13,18]—represent a new generation of contrast agents that show promise for improving signals in reflectance-based diagnostics. Nanoshells consist of a dielectric (silica) core covered by a thin metallic shell. While multilayer nanoshells[16] have been investigated theoretically, construction of such particles has not been achieved. The current study involves nanoshells with a single gold layer. By varying the relative dimensions of core and shell, the optical resonance of these particles can be systematically varied over a broad spectral region from the near-uv to the mid-ir. Therefore, it is possible to engineer gold nanoshells for OCT imaging that have a high level of backscattering and a low level of absorption at the appropriate

---

Address all correspondence to Anant Agrawal, Optical Diagnostics Laboratory, Center for Devices and Radiological Health, US Food and Drug Administration, 12725 Twinbrook Parkway, HFZ-130, Rockville, Maryland 20852; Tel: 301-827-4689; Fax: 301-827-4677; E-mail: anant.agrawal@fda.hhs.gov

1083-3668/2006/11(4)/041121/8/$22.00 © 2006 SPIE

wavelength. Another important property of nanoshells is their ability to be bioconjugated to enzymes and antibodies for selective targeting to receptors of clinical interest.[14,19] In the future, this line of research may lead to an OCT-based molecular imaging approach that is sensitive and specific to neoplastic lesions and provides high levels of contrast.

OCT imaging with gold nanoshells has been documented. Loo et al.[15] compared *in vitro* OCT images of water, microsphere suspension, and nanoshell suspension at an illumination wavelength of 830 nm. The nanoshells used in this study had a silica core diameter of 200-nm and 20-nm shell thickness and were suspended in water at a concentration of $\sim 10^9/\mathrm{mL}$. Experimental data on the influence of specific nanoshell parameters are not yet available in the literature. Such data are needed to elucidate the optical characteristics of these particles and facilitate the development and optimization of nanoshell-enhanced OCT for minimally invasive diagnostics. Therefore, the goal of this study was to quantify the effect of nanoshell core diameter, shell thickness and concentration on the contrast enhancement provided by nanoshells during OCT imaging at 1310 nm.

2 Methods

Optical properties of nanoshells were determined from analytical vector-based solutions to Maxwell's equations for the incident, internal, and scattered electromagnetic fields.[20–22] Briefly, matching the boundary conditions between the core and shell and between the shell and surrounding medium allows coefficients defining the electric and magnetic fields to be determined. These coefficients are dependent on the dielectric constants of the core, shell, and medium, on the core and total nanoshell radii, and on the wavelength. Two of these coefficients, a_n and b_n, define the scattered field and therefore permit direct computation of the extinction, scattering, and backscattering efficiencies (Q_{ext}, Q_{sca}, Q_{back}), as follows[23]:

$$Q_{ext} = \frac{2}{x^2}\sum_{n=1}^{\infty}(2n+1)\,\mathrm{Re}\{a_n + b_n\},$$

$$Q_{sca} = \frac{2}{x^2}\sum_{n=1}^{\infty}(2n+1)(|a_n|^2 + |b_n|^2),$$

$$Q_{back} = \frac{1}{x^2}\left|\sum_{n=1}^{\infty}(2n+1)(-1)^n(a_n - b_n)\right|^2,$$

where x is the size parameter, $2\pi r/\lambda$; r is the total nanoshell radius; and λ is the wavelength in the surrounding medium. Absorption efficiency (Q_{abs}) is then determined from Q_{ext} and Q_{sca}: $Q_{abs}=Q_{ext}-Q_{sca}$. Each optical transport coefficient (μ_x cm^{-1}) is easily computed from its corresponding efficiency (Q_x) by $\mu_x = Q_x \pi r^2 \rho$, where ρ is the volume density of particles (cm^{-3}). At an illumination wavelength of 1310 nm, calculations indicated that nanoshells with a core diameter over 200 nm and shell thickness greater than 15 nm show higher scattering efficiencies. In addition, absorption efficiencies decrease dramatically as shell thickness increases over approximately 15 nm. Thus, nanoshells with these size characteristics were expected to yield strong OCT signal.

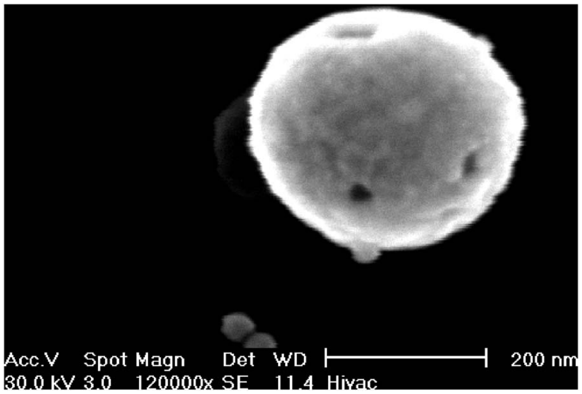

Fig. 1 SEM image of nanoshell with 291-nm core diameter and 15-nm shell thickness.

Nanoshells were fabricated by the authors at Rice University. The fabrication protocol developed for nanoshells includes molecular self-assembly and colloid chemistry in an aqueous solution.[24] For the nanoshell cores, silica nanoparticles were made by the Stöber method, which involves the reduction of tetraethylorthosilicate (Sigma-Aldrich, St. Louis, Missouri) in ethanol. The sizes of the silica cores were determined by scanning electron microscopy (SEM). The cores were functionalized with aminopropyltriethoxysilane (Sigma-Aldrich), resulting in attached amine groups. For the shell, colloidal gold nanoparticles of 1- to 3-nm diameter were fabricated according to the method of Duff et al.[25] This colloidal suspension was first aged for two weeks at 4°C and concentrated using a rotary evaporator. When the functionalized silica cores were placed in the aged colloidal suspension, gold nanoparticles adsorbed to the amine groups. Adsorbed gold provided the nucleation sites for further reduction of gold, until these sites coalesced into a complete shell. The amount of gold added during this final reduction stage determined the shell thickness. Final gold nanoshell sizes were evaluated by SEM. Prior to OCT experiments, nanoshell surfaces were modified with polyethylene glycol (PEG)-thiol to provide steric stabilization as well as to eliminate nonspecific protein adsorption. PEG-thiol was synthesized by reacting 2-iminothiolane (Sigma-Aldrich) with PEG-NH2 5000 MW (Nektar Therapeutics, Huntsville, Alabama). After mixing and reacting equal volumes of the PEG-amine and iminothiolane for 1 h, they were dialyzed against deionized water for 1 to 2 h, changing the dialysate four times in order to remove excess reagent. While initial research indicates that PEGylation can decrease scattering intensity from nanoshells, we investigated only PEGylated nanoshells because these are the most relevant for *in vivo* applications. Nanoshells with six unique geometries were fabricated: (core diameter/shell thickness, in nanometers) 126/15, 126/26, 213/19, 291/8, 291/15, 291/25. Figure 1 shows a SEM image of a 291/15 nanoshell.

Nanoshell concentrations were determined via an approach resembling hemacytometer-based cell counting. Nanoshell suspensions were first diluted by a known factor to achieve $\sim 10^7$ particles/mL. We then captured digital charge-coupled device (CCD) images of each diluted suspension in a 0.1-mm

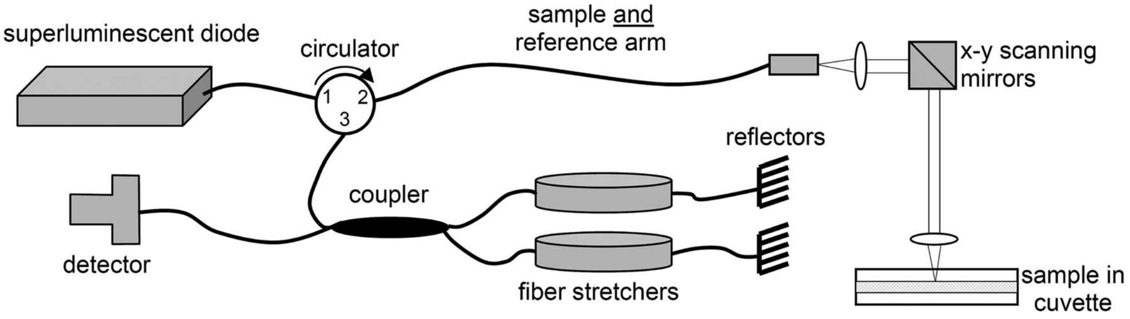

Fig. 2 Diagram of autocorrelator-based OCT system.

pathlength cuvette under a darkfield microscope with a 20× objective. Darkfield microscopy was preferred over brightfield because of substantially better image contrast. The CCD field of view was calibrated (microns/pixel) with a scale having 10-μm rulings; therefore, the volume in the field of view was known. We used our own MATLAB code to locate and tally all the particles in each image and then compute the concentration. The precision of this counting approach, evaluated by counting three samples of each nanoshell suspension, was 12% or better (one standard deviation). The final estimates of nanoshell concentrations were accurate to within 9%, as determined by using the above method to count microsphere suspensions with known concentrations.

Measurements were performed with a time-domain OCT system based on an all-fiber common-path interferometer, also known as an autocorrelator (AIF-INST-02, Optiphase, Van Nuys, California).[26] Sharma et al.[27] have described and analyzed a similar OCT system configuration. A diagram of our system is shown in Fig. 2. As compared to the standard Michelson interferometer, the autocorrelator does not have a separate reference arm and instead derives its reference signal from a reflection in the sample path. Depth ranging is achieved by two piezoelectric fiber stretchers driven by triangular voltage waveforms 180 deg out of phase with each other. This push-pull operation permits depth scans up to 7 mm in air. The OCT sample path consists of the single-mode fiber input/output of the autocorrelator coupled to an 11-mm focal length collimating lens (F220FC-C, Thorlabs, Newton, New Jersey), followed by x- and y-scanning galvanometer mirrors (Model 6210, Cambridge Technology, Cambridge, Massachusetts), and finally a refocusing lens (C280TM-C, Thorlabs) with an 18-mm focal length. Because the fiber has angled faces and the lenses have efficient antireflective coatings, the first possible back reflection that provides the reference signal occurs at the sample itself. To optimize signal-to-noise ratio (SNR), the magnitude of the reference can be adjusted by the type of cover glass (or lack thereof) over the sample and/or by the axial position of the beam focus. The shot noise-limited SNR of the system is 61 dB. The system's decibel intensity units were calibrated by recording the changes in signal intensity from a glass plate as the light source output power, measured with a U.S. National Institute of Standards and Technology–traceable power meter, was varied over two orders of magnitude. The light source for this OCT system is a superluminescent diode centered at 1310 nm with a 50-nm spectral bandwidth, which therefore yields a coherence length of 17 μm in air. The lateral resolution is 15 μm at focus, and the optical power at the sample is approximately 12 mW.

OCT measurements were taken of the nanoshells in water and turbid, tissue-simulating phantoms. The phantoms consisted of 1.53-μm diameter polystyrene microspheres (Polysciences, Warrington, Pennsylvania) suspended in water. These phantoms had a scattering coefficient (μ_s) of 100 cm^{-1} and anisotropy of 0.9, based on Mie theory calculations. This level of scattering is directly relevant to biological tissue at 1310 nm.[28] Samples were imaged in a 0.5- or 1-mm pathlength two-piece cuvette, with the OCT beam axially focused at the interface between the cuvette glass and liquid sample, to maximize signal, and hence SNR, from the sample itself. Each B-scan image required 3 s of acquisition time and consisted of 120 A-scans taken at 40 Hz over a 0.85-mm lateral region. To ensure a homogeneous distribution of particles, each suspension was agitated just prior to OCT imaging. The particle settling time was analyzed and found to produce noticeable changes in the OCT signal about 45 s after ceasing agitation. Therefore, each B-scan was acquired within 15 s of agitation. Figures 3(a) and 3(b) show typical B-scan images of water and nanoshells in water. To reduce the effects of speckle and to obtain more reliable intensity estimates at low nanoshell concentrations, all 120 A-scans from each B-scan were averaged for subsequent analysis.

Two sets of measurements were performed in this study. The first set involved OCT imaging of nanoshells in water and phantom solutions where the concentration of nanoshells in each sample was held constant at 5×10^9 particles/mL. In the second set of measurements, we investigated the effect of nanoshell concentration on OCT signal intensity in water and phantom. Each data point displayed in the figures represents the mean of three measurements. The standard deviation for each data point was also computed, but the error bars on each graph represent the maximum standard deviation of all points on that graph.

3 Results

The intent of the first set of measurements was to determine the intensity gain achieved by the addition of nanoshells with differing geometries. Intensity gain was defined as the average intensity over the first 100 μm of a sample (water or phantom) with nanoshells minus the corresponding average intensity of that sample without nanoshells. The averaging was

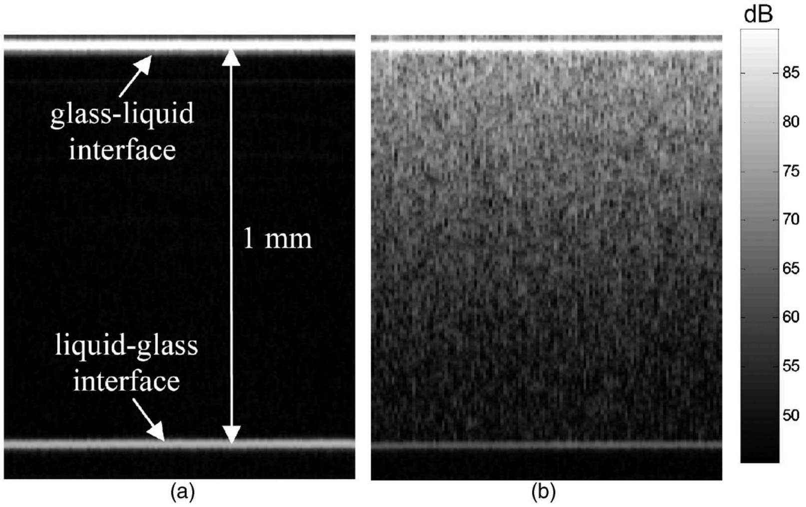

Fig. 3 OCT B-scan images of 1-mm pathlength cuvette filled with (a) water and (b) 291/25 nanoshells at a concentration of 5×10^9 particles/mL in water.

limited to the first 100 μm beyond the glass-liquid interface (75 to 175 μm from the peak) to minimize the effect of signal attenuation. For the case of nanoshells added to water, a graph of average A-scans for two nanoshell types and a water baseline is shown in Fig. 4(a). Figure 4(b) shows the intensity gain values for all the nanoshells added to water. This graph shows a variation of intensity gains from 19 to 28 dB in a monotonic relationship with the predicted backscattering coefficient (μ_{back}). As expected, larger core and shell sizes tended to generate higher levels of backscattering and thus greater intensity gain. Note that the nanoshells with the largest core but smallest shell (291/8) produced a smaller signal than those with smaller core and larger shell (213/19).

Figures 5(a) and 5(b) are analogous to Figs. 4(a) and 4(b), but here nanoshells are added to the microsphere-based turbid phantom and intensity gains are computed relative to the phantom alone. Average A-scan data are shown in Fig. 5(a). Average intensity gains shown in Fig. 5(b) vary from 2 to 7 dB, in a monotonic relationship with the predicted μ_{back}. The level of intensity gain produced by nanoshells in the phantom material is much lower than that seen for the water-based measurements. We can interpret the intensity gains seen with this phantom as a meaningful prediction of actual intensity gains to be expected when these nanoshells are added to tissue.

The OCT signal attenuation due to nanoshells was measured in water using the intensity of the reflection from the liquid-glass interface at the bottom of a 1-mm pathlength cuvette. This interface was used to quantify attenuation because it provided a strong signal that was more easily quantifiable and had lower error levels than calculating the attenuation by the standard approach of fitting the decay curve. Given the relatively small variations in OCT signal attenuation with nanoshell parameters, this strong signal was necessary to provide an accurate illustration of changes in attenuation. The drop in this intensity when the nanoshells were added to water provides the attenuation value, as shown in Fig. 6(a). Note that in this graph, the attenuation in the turbid phantom is much greater than that of the nanoshells, as indicated both by the rate of signal decay as well as the size of the second peak (or lack thereof, in the phantom case). The lack of a first order decay in the phantom indicates a significant contribution of multiply scattered light.[29] Figure 6(b) shows that the measured attenuation in water tracks the predicted extinction co-

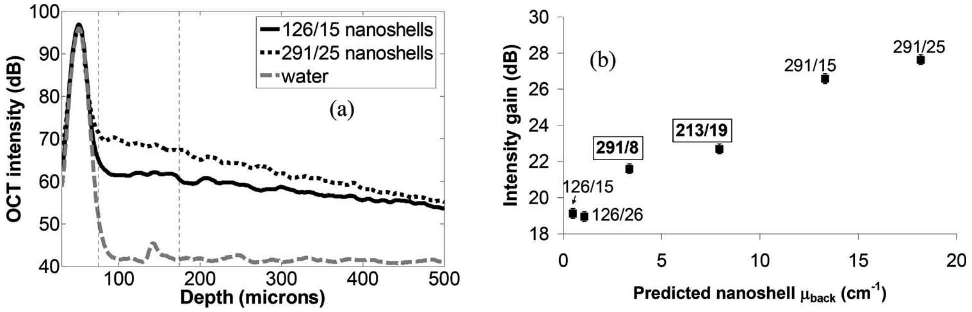

Fig. 4 (a) Average A-scans of water and two different sizes of nanoshells in water (5×10^9 nanoshells/mL). The vertical dotted lines indicate the first 100 μm over which the intensity was averaged for intensity gain estimates. (b) Measured intensity gain from each size of nanoshells versus the backscattering coefficient (μ_{back}) predicted for each size of nanoshells. Note that data points are labeled with core diameter/shell thickness in nanometers.

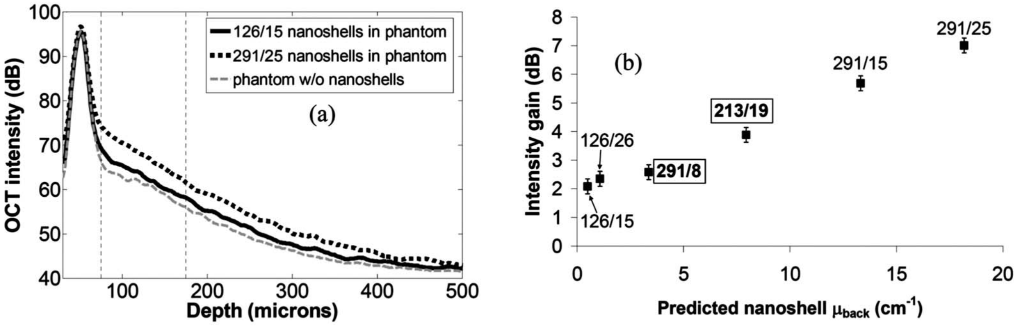

Fig. 5 (a) Average A-scans of a tissue phantom and two different sizes of nanoshells in the phantom (5×10^9 nanoshells/mL). The vertical dotted lines indicate the first 100 μm over which the intensity was averaged for intensity gain estimates. (b) Measured intensity gain from each size of nanoshells versus the backscattering coefficient (μ_{back}) predicted for each size of nanoshells.

efficient (μ_{ext}) of nanoshells. In this graph, the order of the 213/19 and 291/8 nanoshells has reversed as compared to the intensity gain, because the thin shell of the 291/8 nanoshells leads to increased absorption. These results indicate that nanoshells with larger core and shell have a greater potential for inducing attenuation; however, this attenuation was minimal compared to that produced by the phantom.

A more biologically relevant evaluation of attenuation was performed by measuring changes due to nanoshells in a turbid phantom. However, due to the high attenuation of the phantom—and subsequent absence of a significant sample-glass interface peak—it was not possible to use the same setup as for the attenuation measurements in water. Two changes were made to our approach in order to enable a measurable peak: (1) the pathlength of the sample region was decreased to 0.5 mm, and (2) a mirror was used as the bottom surface of the two-piece cuvette. This setup allowed us to observe that the attenuation of the phantom alone is 54 dB (relative to water). Figure 7 shows the additional attenuation caused by each type of nanoshells in the phantom. The trend in this graph is similar to that seen in Fig. 6(b), though the level of attenuation is reduced.

Optimization of nanoshell-enhanced OCT will require a quantitative understanding of the influence of nanoshell concentration. To address this issue, we measured the intensity gain from three types of nanoshells at various concentrations in a scattering phantom. The nanoshell geometries chosen for this analysis—126/15, 213/19, 291/25—provide insight into the range of OCT signal intensity gains that can be produced for a given concentration. The intensity gain was determined in a similar manner as for Figs. 4(b) and 5(b), by computing the average intensity over the first 100 μm of an average A-scan. Results in Fig. 8 show a strong increase in intensity gain with concentration for each of the three nanoshells. For all nanoshell types, the intensity gain did not rise appreciably above the noise floor for concentrations less than 5×10^8 nanoshells/mL. As expected, the 291/25 nanoshells produced the greatest intensity gain at all concentrations over which signals were above the noise floor. Setting the threshold for detection at a level slightly above the noise floor (2 dB), the minimum concentrations required to produce threshold-level intensity gains were 10^{10}, 2×10^9, and 10^9 nanoshells/mL for the 126/15, 213/19, and 291/25 geometries, respectively. At any particular concentration level, the trends in intensity gain as a function of nanoshell type are in agreement with results in Figs. 4(b) and 5(b).

4 Discussion

Prior studies have established the ability of nanoshells to provide improved contrast during OCT imaging of biological tissues. This work, however, represents the first parametric experimental investigation of the factors that influence signal enhancement by nanoshells. The *in vitro* phantom measurements performed in this study provide unique insights into the OCT imaging characteristics of nanoshells. With this informa-

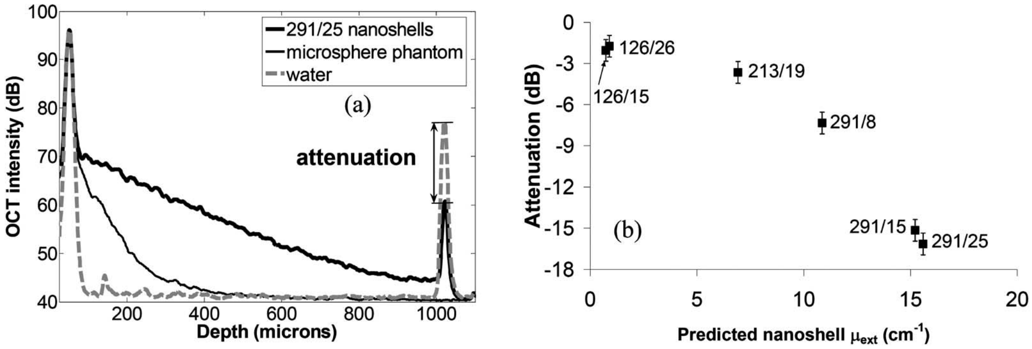

Fig. 6 (a) Average A-scans of water, a turbid tissue phantom and nanoshells in water (5×10^9 nanoshells/mL). The cuvette pathlength is 1 mm. (b) Measured attenuation from each size of nanoshells in water as a function of the nanoshell extinction coefficient (μ_{ext}) predicted from theory.

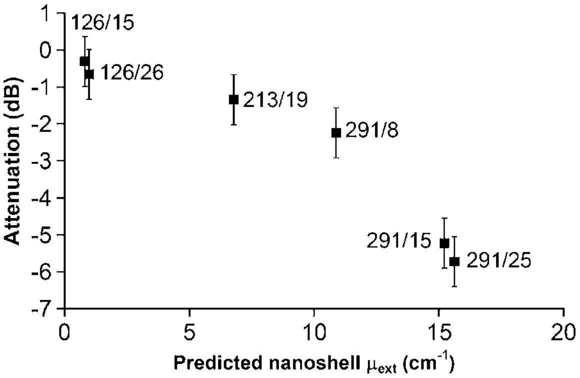

Fig. 7 Measured incremental attenuation due to several sizes of nanoshells (5×10^9 nanoshells/mL) in a turbid tissue phantom as a function of the nanoshell extinction coefficient (μ_{ext}) predicted from theory. The cuvette pathlength used here is 0.5 mm.

tion, it is now possible to begin a rigorous analysis of the issues related to optimization of nanoshell parameters for *in vivo* diagnosis.

Our experimental results provide evidence that increases in core diameter over the range of 126 to 291 nm and shell sizes over the range of 8 to 25 nm can produce a significant increase in OCT signal intensity at 1310 nm. The turbid phantom alone generated an intensity level of about 20 dB above the noise floor. As indicated by Fig. 5(b), 5-dB intensity gains at a nanoshell concentration of 5×10^9 nanoshells/mL were possible by increasing core diameter (126/26 to 291/25) or shell thickness (291/8 to 291/25). The highest intensity gain generated in a phantom was a value of 9 dB (Fig. 8). This gain was produced for the 291/25 nanoshells at a concentration of 10^{10} nanoshells/mL.

While these results indicate that achieving large increases in the OCT signal necessitates a large core diameter and shell thickness, these same attributes can also result in greater signal attenuation. Our experimental results indicate that for all but the nanoshells with the largest overall sizes, attenuation was relatively minimal. The 291/25 nanoshells at a concentration of 5×10^9 nanoshells/mL produced nearly 6 dB of attenuation over a 0.5-mm pathlength. Although 6 dB is relatively small compared to the 54 dB of attenuation produced by the turbid phantom, nanoshell attenuation might become significant over greater depths, particularly in tissues with low attenuation levels and for cases in which nanoshell concentrations are significantly greater than those investigated here. It is worthwhile noting that, according to the calculated optical properties, the relative contribution of scattering to the total attenuation increases dramatically with core diameter and shell thickness. For example, in the case of 126/15 nanoshells, absorption is 1.5 times stronger than scattering; whereas, for the 291/25 geometry, scattering is more than 5 times as strong as absorption.

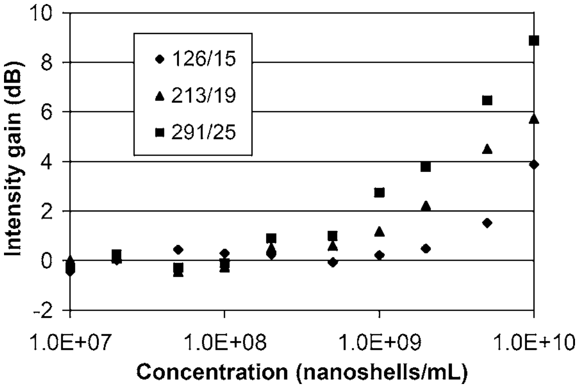

Fig. 8 Measured intensity gain as a function of nanoshell type and concentration. Data are shown for three different nanoshell types added to a turbid tissue phantom. Maximum standard deviation ($n = 3$) was 0.8 dB. Error bars are not shown for clarity.

Variations in the intensity gain and attenuation as a function of shell thickness were less consistent than those seen for core diameter. For nanoshells with a core diameter of 291 nm, the change in predicted μ_{back} was sixfold as shell diameter increased from 8 to 25 nm and the increase in experimentally measured intensity gain in the turbid phantom was 4.4 dB. However, in three cases, minimal differences were seen between results for nanoshells with the same core diameter but different shell thickness. One instance involves the intensity gain data for 126/15 and 126/26 nanoshells [Figs. 4(b) and 5(b)]. The other two cases involve attenuation data for the 126/15 and 126/26 nanoshells as well as the 291/15 and 291/25 nanoshells [Figs. 6(b) and 7]. The changes in backscattering and attenuation over these ranges were too small to be detected by our OCT system. Although variations in nanoshell parameters do not induce consistent, linear variations in backscattering or attenuation, the trends seen in the measurements match those from the calculated optical properties.

Prior calculations for a wavelength of 830 nm indicated that scattering increases monotonically with shell thickness, but varies in an irregular, nonmonotonic manner with nanoshell core diameter.[15] At 1310 nm, however, theoretical results indicate monotonic, albeit nonlinear, increases in scattering efficiency with both core and shell size. Not only do our results corroborate the trends expected from varying each of these two geometric parameters but also for the combined effect of the parameters as well. As indicated in Figs. 4 and 5, intensity gain increased as predicted when one parameter was held constant and the other was increased. While the predominant effect was an increase in intensity gain with core size, results clearly indicate one case in which the smaller core nanoshells (213/19) produced more signal than ones with larger core (291/8). This was due to the thicker shell of the 213/19 nanoshells and is in agreement with theory. While a fully quantitative validation of calculated optical properties will be performed in a future study, our current results provide strong corroboration with theoretically predicted trends.

One of the most important practical concerns for nanoshell-based enhancement of OCT images is the density or concentration of nanoshells that are necessary to produce a reliably detectable level of contrast. A series of measurements at different concentrations (Fig. 8) provides insight into the issue of detection threshold. As expected, nanoshells with higher backscattering efficiencies required lower concentrations to reach the detection threshold. For the most highly backscattering nanoshells (291/25), a concentration of 10^9

nanoshells/mL was required to produce an intensity gain of 2 dB or more in the phantom.

We can compare this threshold concentration of 10^9 nanoshells/mL to what concentrations may be realized in cancerous tumors *in vivo*. First, we consider the case of nanoshells labeled to target a tumor. A tumor marker such as the epidermal growth factor receptor can be found at levels of 10^6 per cell on cancerous cells (versus 10^3 to 10^5 per cell on normal cells).[30,31] For the case of cells with 10-μm diameter and nanoshells with 300-nm diameter, then up to 4000 nanoshells could be accommodated on the cell surface, and at least 100 receptors would be available to bind to each antibody-conjugated nanoshell. If only 10% of each cell's surface were covered with nanoshells (400 nanoshells/cell), the nanoshell concentration would be 6.4×10^{11} nanoshells/mL, two orders of magnitude above the threshold concentration.

In addition to a molecularly specific mechanism of delivering nanoshells to a tumor, there is also an opportunity for intravenously injected, unlabeled nanoshells to accumulate in a tumor via passive extravasation from its leaky vasculature.[32–34] However, there is limited information in the literature to precisely predict the potential concentration of unlabeled nanoshells accumulating in a tumor in this manner. Unezaki et al.[34] found that $\sim 15\%$ of an intravenously injected 1-mg dose of PEG-coated liposomes (198-nm mean diameter) would accumulate in 1-g tumors inoculated subcutaneously in mice. Assuming the tissue and liposome mass densities are similar to that of water $(1\ \mathrm{g/cm^3})$, then a final concentration of 3.7×10^{10} particles/mL accumulated in each tumor, again well above the nanoshell threshold concentration. Interestingly, there was a distinct size dependence of the extravasation, with 63-nm and 388-nm diameter liposomes showing significantly less accumulation than the 198-nm liposomes.

Given the results presented here on the variations in nanoshell optical performance, it is useful to consider what geometry is optimal for OCT imaging, or perhaps more importantly, what factors should be considered in determining whether a nanoshell is "optimal." Because a high OCT signal level would facilitate detection, one criteria is maximum intensity gain. Within the range of parameters that were investigated in the current study, the nanoshell with the largest core (291-nm diameter) and shell (25-nm thick) provided maximum OCT signal enhancement. However, this nanoshell also produced the greatest attenuation of OCT signals. Whether or not this attenuation is significant would depend on both the distribution and concentration of the nanoshells. For the nanoshell concentrations investigated here, attenuation was much less than that of biological tissue. Therefore, the contribution to overall signal loss would likely be minimal unless the nanoshells were present in very high concentrations and/or at moderately high concentrations throughout the entire depth being scanned. On the other hand, if a highly concentrated grouping of nanoshells was present at a targeted tumor, significant localized attenuation might be produced, causing strong shadowing in the region below the tumor. This shadowing, combined with a high level of backscatter, might lead to improved detection of tumors.

While 291/25 nanoshells produced the greatest signal for a given concentration, they may not be the best choice for all OCT applications. In addition to the studies of passive extravasation discussed earlier, there is further evidence that the pharmacokinetics of nanoshells is dependent on particle size—specifically, larger particles may suffer from limited or slow biodistribution and clearance.[35] Furthermore, if the amount of nanoshells delivered is limited by volume rather than particle concentration (e.g., due to safety concerns), smaller diameter nanoshells may actually be more effective at producing high OCT signals. Results in Fig. 8 indicate that the concentration of nanoshells required to achieve an intensity gain of about 4 dB using 291/25 nanoshells is one-fifth that required when using 126/15 nanoshells. However, the volume of a 291/15 nanoshell is about 10 times greater than that of a 126/15 nanoshell. Therefore, 126/15 nanoshells—the smallest nanoshells tested in this study—would likely produce more signal per nanoshell volume.

5 Conclusion

The influence of nanoshell geometry and concentration on OCT signal enhancement in turbid media was investigated through *in vitro* OCT measurements. Nanoshells with core diameters of 126 to 291 nm and shell thicknesses of 8 to 25 nm were studied in water and turbid tissue phantoms. Monotonic increases of up to 8 dB in OCT intensity gain and 6 dB in signal attenuation were found with increasing core and shell size for concentrations of 5×10^9 nanoshells/mL. These gains were not linear with either geometric parameter yet were qualitatively consistent with calculated optical properties. Results indicate that a concentration of 10^9 nanoshells/mL may be needed to provide meaningful (2 dB) signal enhancement in a relatively homogeneous turbid medium. These results help elucidate a number of basic issues relevant to optimization of nanoshell parameters for reflectance-based diagnostics and will facilitate future studies toward the development of a viable molecular OCT imaging approach.

Acknowledgments

The authors acknowledge support from the Welch Foundation, Beckman Foundation, and the National Science Foundation Center for Biological and Environmental Nanotechnology at Rice. We also acknowledge Jeff Bush of Optiphase, Inc. for many helpful discussions on configuring and characterizing our autocorrelator.

The opinions and conclusions stated in this paper are those of the authors and do not represent the official position of the U.S. Food and Drug Administration. The mention of commercial products, their sources, or their use in connection with material reported here is not to be construed as either an actual or implied endorsement of such products by the U.S. Food and Drug Administration.

References

1. D. Huang, E. A. Swanson, C. P. Lin, J. S. Schuman, W. G. Stinson, W. Chang, M. R. Hee, T. Flotte, K. Gregory, C. A. Puliafito, and J. G. Fujimoto, "Optical coherence tomography," *Science* **254**, 1178–1181 (1991).
2. J. K. Barton, J. B. Hoying, and C. J. Sullivan, "Use of microbubbles as an optical coherence tomography contrast agent," *Acad. Radiol.* **9**, S52–S55 (2002).

3. T. M. Lee, A. L. Oldenburg, S. Sitafalwalla, D. L. Marks, W. Luo, F. J. Toublan, K. S. Suslick, and S. A. Boppart, "Engineered microsphere contrast agents for optical coherence tomography," *Opt. Lett.* **28**(17), 1546–1548 (2003).
4. C. Xu, J. Ye, D. L. Marks, and S. A. Boppart, "Near-infrared dyes as contrast-enhancing agents for spectroscopic optical coherence tomography," *Opt. Lett.* **29**(14), 1647–1649 (2004).
5. Y. Yang, P. O. Bagnaninchi, S. C. Whiteman, D. G. van Pittius, A. J. El Haj, M. A. Spiteri, and R. K. Wang, "A naturally occurring contrast agent for OCT imaging of smokers' lung," *J. Phys. D* **38**, 2590–2596 (2005).
6. A. L. Oldenburg, J. R. Gunther, and S. A. Boppart, "Imaging magnetically labeled cells with magnetomotive optical coherence tomography," *Opt. Lett.* **30**(7), 747–749 (2005).
7. C. Yang, "Molecular contrast optical coherence tomography: a review," *Photochem. Photobiol.* **81**, 215–237 (2005).
8. S. A. Boppart, A. L. Oldenburg, C. Xu, and D. L. Marks, "Optical probes and techniques for molecular contrast enhancement in coherence imaging," *J. Biomed. Opt.* **10**(4), 41208 (2005).
9. K. D. Rao, M. A. Choma, S. Yazdanfar, A. M. Rollins, and J. A. Izatt, "Molecular contrast in optical coherence tomography by use of a pump-probe technique," *Opt. Lett.* **28**(5), 340–342 (2003).
10. C. Yang, L. E. McGuckin, J. D. Simon, M. A. Choma, B. E. Applegate, and J. A. Izatt, "Spectral triangulation molecular contrast optical coherence tomography with indocyanine green as the contrast agent," *Opt. Lett.* **29**(17), 2016–2018 (2004).
11. C. Yang, M. A. Choma, L. E. Lamb, J. D. Simon, and J. A. Izatt, "Protein-based molecular contrast optical coherence tomography with phytochrome as the contrast agent," *Opt. Lett.* **29**(12), 1396–1398 (2004).
12. J. S. Bredfeldt, C. V. Vinegoni, D. L. Marks, and S. A. Boppart, "Molecularly sensitive optical coherence tomography," *Opt. Lett.* **30**(5), 495–497 (2005).
13. H. Cang, T. Sun, Z. Li, J. Chen, B. J. Wiley, Y. Xia, and X. Li, "Gold nanocages as contrast agents for spectroscopic optical coherence tomography," *Opt. Lett.* **30**(22), 3048–3050 (2005).
14. K. Sokolov, M. Follen, J. Aaron, I. Pavlova, A. Malpica, R. Lotan, and R. Richards-Kortum, "Real-time vital optical imaging of precancer using anti-epidermal growth factor receptor antibodies conjugated to gold nanoparticles," *Cancer Res.* **63**, 1999–2004 (2003).
15. C. H. Loo, A. W. H. Lin, M. Lee, J. K. Barton, N. J. Halas, J. L. West, and R. A. Drezek, "Nanoshell-enabled photonics-based imaging and therapy of cancer," *Technol. Cancer Res. Treat.* **3**, 33–40 (2004).
16. K. Chen, Y. Liu, G. Ameer, and V. Backman, "Optimal design of structured nanospheres for ultrasharp light-scattering resonances as molecular imaging multilabels," *J. Biomed. Opt.* **10**, 024005 (2005).
17. A. W. H. Lin, N. A. Lewinski, J. L. West, N. J. Halas, and R. A. Drezek, "Optically tunable nanoparticle contrast agents for early cancer detection: model-based analysis of gold nanoshells," *J. Biomed. Opt.* **10**, 064035 (2005).
18. J. Chen, F. Saeki, B. J. Wiley, H. Cang, M. J. Cobb, Z. Y. Li, L. Au, H. Zhang, M. B. Kimmey, X. Li, and Y. Xia, "Gold nanocages: bioconjugation and their potential use as optical imaging contrast agents," *Nano Lett.* **5**(3), 473–477 (2005).
19. C. Loo, L. Hirsch, M. Lee, E. Chang, J. L. West, N. J. Halas, and R. A. Drezek, "Gold nanoshell bioconjugates for molecular imaging in living cells," *Opt. Lett.* **30**(9), 1012–1014 (2005).
20. D. Sarkar and N. J. Halas, "General vector basis function solution of Maxwell's equations," *Phys. Rev. E* **56**, 1102–1112 (1997).
21. S. J. Oldenburg, "Light scattering from gold nanoshells," Ph.D dissertation, Rice University (1999).
22. A. L. Aden and M. Kerker, "Scattering of electromagnetic waves from two concentric spheres," *J. Appl. Phys.* **22**, 1242–1246 (1951).
23. C. F. Bohren and D. R. Huffman, *Absorption and Scattering of Light by Small Particles*, Wiley, New York (1983).
24. S. L. Westcott, J. B. Jackson, C. Radloff, and N. J. Halas, "Relative contributions to the plasmon lineshape of metal nanoshells," *Phys. Rev. B* **66**, 155431 (2002).
25. D. G. Duff, A. Baiker, and P. P. Edwards, "New hydrosol of gold clusters. 1. Formation and particle size variation," *Langmuir* **9**, 2301–2309 (1993).
26. J. Bush, P. Davis, and M. A. Marcus, "All-fiber optic coherence domain interferometric techniques," *Proc. SPIE* **4204**, 71–80 (2000).
27. U. Sharma, N. Fried, and J. Kang, "All-fiber common-path optical coherence tomography: sensitivity optimization and system analysis," *IEEE J. Sel. Top. Quantum Electron.* **11**(4), 799–805 (2005).
28. T. Troy and S. N. Thennadil, "Optical properties of human skin in the near infrared wavelength range of 1000 to 2200 nm," *J. Biomed. Opt.* **6**(2), 167–176 (2001).
29. R. K. Wang, "Signal degradation by multiple scattering in optical coherence tomography of dense tissue: a Monte Carlo study towards optical clearing of biotissues," *Phys. Med. Biol.* **47**, 2281–2299 (2002).
30. T. T. Kwok and R. M. Sutherland, "Differences in EGF related radiosensitisation of human squamous carcinoma cells with high and low numbers of EGF receptors," *Br. J. Cancer* **64**(2), 251–254 (1991).
31. G. Carpenter, "Receptors for epidermal growth factor and other polypeptide mitogens," *Annu. Rev. Biochem.* **56**, 881–914 (1987).
32. H. Maeda, J. Fang, T. Inutsuka, and Y. Kitamoto, "Vascular permeability enhancement in solid tumor: various factors, mechanisms involved and its implications," *Int. J. Immunopharmacol* **3**, 319–328 (2003).
33. O. Ishida, K. Maruyama, K. Sasaki, and M. Iwatsuru, "Size dependent extravasation and interstitial localization of polyethyleneglycol liposomes in solid tumor-bearing mice," *Int. J. Pharm.* **190**, 49–56 (1999).
34. S. Unezaki, K. Maruyama, J. Hosoda, I. Nagae, Y. Koyanagi, M. Nakata, O. Ishida, M. Iwatsuru, and S. Tsuchiya, "Direct measurement of the extravasation of polyethyleneglycol-coated liposomes into solid tumor tissue by *in vivo* fluorescence microscopy," *Int. J. Pharm.* **144**, 11–17 (1996).
35. G. L. McIntire, E. R. Bacon, K. J. Illig, S. B. Coffey, B. Singh, G. Bessin, M. T. Shore, and G. L. Wolf, "Time course of nodal enhancement with CT X-ray nanoparticle contrast agents: effect of particle size and chemical structure," *Invest. Radiol.* **35**(2), 91–96 (2000).